Received: 12 September 2022 | Accepted: 10 June 2023

DOI: 10.1111/1365-2478.13393

Geophysical Prospecting | EAGE EUROPEAN ASSOCIATION OF GEOSCIENTISTS & ENGINEERS

ORIGINAL ARTICLE

Sparse-node acquisition for data fitting velocity model building

Denes Vigh | **James Xu** | **Xin Cheng** | **Kate Glaccum**

SLB, Houston, Texas, USA

Abstract

The salt interpretation can be quite time-intensive and challenging. Full-waveform inversion, as a data-driven optimization algorithm with full wavefield modelling, has become one of the essential tools for earth model building. However, full-waveform inversion application in the complex salt geology, especially with streamer data collection, is limited, whereas the ocean-bottom node with ultra-long offsets and low frequencies unleashes the power of full-waveform inversion. Sparse ocean-bottom node acquisition has become a standard approach to improve the earth model building by the addition of ultra-long offsets and possibly low frequencies. The new survey designs with ocean-bottom node coupled with simultaneous shooting can be deployed on a regional basis covering thousands of square kilometres in a cost-effective manner. In complex geological settings, including irregular salt geometry, salt interpretation has a direct impact on subsalt imaging. The recent development of robust objective functions allows full-waveform inversion work with sparse ocean-bottom node surveys in the deep-water environment as the Gulf of Mexico to build and refine the salt geometries and correct the background velocity error in subsalt, uncovering the structural configuration of the basin that has not been seen before. Although full-waveform inversion mostly employs the acoustic wave equation, we know that the high velocity boundaries in the earth model may require elastic wavefield propagation. Increased physics in full-waveform inversion allows us to interrogate the power of elastic full-waveform inversion versus acoustic full-waveform inversion, and here, we demonstrate that elastic full-waveform inversion has an advantage over acoustic full-waveform inversion despite the extra cost associated with implementing the more complete physics.

KEYWORDS

acoustics, acquisition, elastics, full waveform, inversion

INTRODUCTION

In the last 30 years, large oil reserves have been discovered in the deep-water Gulf of Mexico based on seismic data. The main challenges for seismic exploration in this region in terms of acquisition were related to subsalt reservoir illumination, as this data requires a wide range of azimuths and long- or very-long-offset distribution. Multiple attenuation, velocity model building and depth imaging accuracy were the main challenges for signal processing and imaging. Significant progress was made in acquisition and data processing during the last 15 years to solve these problems. However, imaging subsalt targets has been a major obstacle due to the complex salt geometries in the overburden. Previously, substantial improvement in subsalt illumination was achieved using innovative towed-streamer, wide and/or full azimuthal acquisition designs with increasingly longer offsets up to 18–20 km. However, velocity model building has been lagging due to the lack of an automatic method of generating earth models in areas of salt. Full-waveform

inversion (FWI) is a full-wave, propagation-based inversion technique. It has emerged as a promising method for refining detailed seismic velocity fields, which will then benefit from migration techniques to achieve enhanced subsurface images. The algorithm iteratively updates the subsurface earth models to reduce the misfit function, measuring the difference between the recorded seismic data and the simulated waveforms, such that the full waveform (primary, multiples and others) of acquired seismic data can be explained by the inverted subsurface earth models.

It is known that the lack of ultra-low frequencies in the acquired data leads to difficulty recovering the structures especially salt geometries and therefore to the starting-model dependence of FWI (see, e.g. Virieux & Operto, 2009).

In complex salt environments, we have struggled to generate adequate velocity models despite many years of effort. In our experience, the geometry with its 8-km maximum offset produces relatively high wavenumber updates and, in the deep part of the model, we must bring out the low wavenumber of the kernel either implicitly or explicitly, using either the energy norm (Rocha et al., 2016) or Born-modelling approaches (Vigh et al., 2016; Xu et al., 2012). There has been attempts to build salt geometries from sediment only velocity model using reflected data in the FWI (Kalita et al., 2019) which has been proven in synthetic data examples. Fichtner and Trampert (2011) discussed a method computing of the space-dependent parameters via Fourier transform of the Hessian which can improve the convergence of FWI especially in salt related geology. Some approaches advocate using envelope fluctuation and decay of seismic record carries the ultra-low frequency information which may be beneficial building the background model without having low frequencies in the recorded data (Wu et al., 2014).

FWI greatly benefits from long-offset and full-azimuth data, which could drive the update down to the basement and modify the salt geometry to meet the requirements of oil and gas exploration. Deep-water subsalt fields and prospects typically have seismic imaging challenges, and significant effort has been invested over the last few decades to overcome these challenges. Several successful case studies have proven the advantages of FWI with dense ocean-bottom node (OBN) data with node spacings of 200–400 m (Nolte et al., 2019; Li et al., 2019). However, these surveys were limited to focused reservoir imaging and monitoring due to the high operational costs of acquisition.

In the last few years, however, the economics of OBN technology have improved by addressing inefficiencies, including longer node battery life and faster deployment/retrieval methods, such as dual remote-operated vehicle operation. Geometries using increased node spacing allowed this acquisition method to be extended to regional sizes and, specifically, to enable FWI for velocity modelling. In order to further improve acquisition efficiency, sparse OBN surveys were designed and acquired with node interval of 1.2 km, both, along and perpendicular to the node line with 50 km maximum offsets (Vigh et al., 2020).

Besides the complex salt geometry, the long offsets can pose a possible cycle-skipping problem, even though the frequencies available are becoming lower and lower. We developed a robust objective function for this purpose to overcome the possible cycle-skipping named enhanced template matching.

In this paper, we present a case study of FWI applied to a sparse-node acquisition in the Gulf of Mexico, demonstrating the power of FWI in building velocity models, and the much-improved image with the FWI model. Furthermore, if the FWI-predicted data is simulated with an acoustic engine, it could pose amplitude discrepancies at high velocity contrast interfaces and miss the amplitude versus offset effect in certain cases. Recent computer hardware improvements have allowed us to simulate elastic data in a 3D manner and undertake the challenge of executing 3D elastic FWI (EFWI). We demonstrate the FWI progress of the last decade with latest examples from different acquisition geometries. Although hydrophone measurement might be capable of contributing to the shear (S) velocity estimation, the weak converted S wave information presented in the pressure component of towed-streamer data requires a multi-component dataset to derive the shear velocity update. In spite of the computational cost, time-domain EFWI was first successfully applied demonstrated the ability of applying EFWI on multi-component real data by Crase et al. (1990), Sears et al. (2010) in the North Sea and by Djikpéssé and Tarantola (1999) in the GoM. The FWI can be implemented in time-domain or frequency-domain (Brossier, 2010), whereas Castellanos et al. (2011) suggested a hybrid method using time-domain forward modelling with a frequency-domain solver. Huang et al. (2020) introduced an estimation of the uncertainties of the elastic parameters in Bayesian anisotropic EFWI by using Kalman filter with Green's functions.

GEOLOGICAL DESCRIPTION

Herein, we review a case study of approximately 3000 km^2 area situated within the Green Canyon Protraction Area, located 150 km from Port Fourchon, in water depths ranging from 300 to 1200 m. This north-central area within the deep-water Gulf of Mexico is interpreted to have a salt tectonic history, creating a complex structural framework ideal for subsurface exploration. In contrast to regions further south, the allochthonous salt bodies in the case study area are less extensive and more isolated. Remaining salt bodies are separated, at times, by poorly imaged and, thus, heavily interpreted salt weld network with deep mini-basins of thick Pliocene to Pleistocene sediments. Deep salt feeders or salt ascension

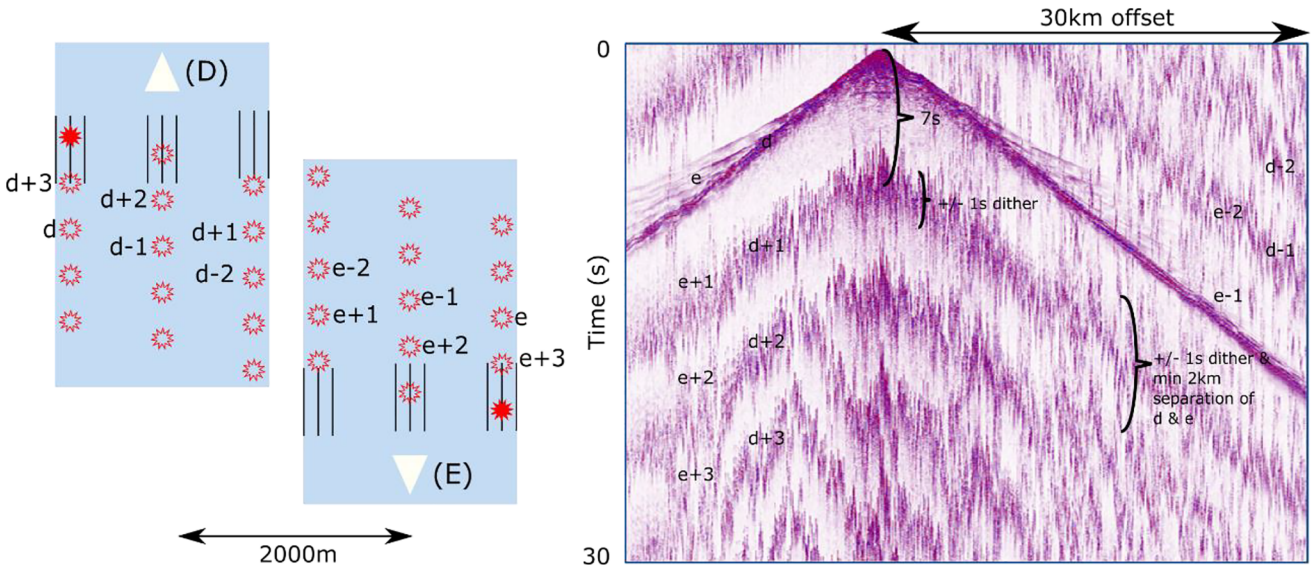

FIGURE 1 The shooting configuration and an example of a common-node record with the simultaneous source interference.

zones are suggested on legacy seismic volumes but are difficult to map with confidence. These salt feeders and deep welds separate the primary basin stratigraphy into multiple sub-basins, each with a different depositional and structural history that can lead to significant variations in velocity. Exploration potential remains unproven beneath salt with only a small number of wells having been drilled to test deeper objectives. The lack of deep well control leads to high uncertainty in sediment velocities below salt. The primary obstacles to identifying and maturing subsalt prospects are the high uncertainty in key structural relationships, and inability to delineate sediment transport fairways, mainly due to the poor seismic imaging at deeper depths.

SPARSE-NODE ACQUISITION PARAMETERS

Model building with full-waveform inversion (FWI) enables relaxing of the acquisition parameters for ocean-bottom node (OBN) surveys, especially the node spacing even in complex salt environments. A sparser node distribution enables a significant cost reduction for these surveys.

Hence, we need to assess the maximum receiver spacing that is acceptable to perform reliable FWI at frequencies up to 15–20 Hz. The upper limit of 15–20 Hz can be explained due to minimal kinematic change in imaging beyond this resolution (Plessix et al., 2021; Ratcliffe et al., 2019). Sparse receiver designs are enabled as the sparse long-offset node acquisition is used independently for the velocity model building by FWI, in contrast to the existing towed-streamer data, which was acquired for reflectivity imaging using reverse-time migration (RTM). The towed-streamer and sparse-node data can then be combined for imaging.

The sparse-node acquisition presented in this case study encompasses a 1.2 km distance between the nodes, and, altogether, 2066 nodes were deployed. Acquisition comprised a 50 m in-line and 100 m crossline shot carpet with a generally 18 km halo around the nodes, giving a natural bin size of 25 m × 50 m. Data was acquired by two vessels with triple sources, using a flip-flap-flop shooting method, with a random ±1000 ms dither applied to each shot, acquired using continuous recording. Each vessel acquired three source lines simultaneously, with a shotpoint spacing of 16.7 m that translates to a ∼7 s time interval. The vessels maintained a minimum 2 km separation and were generally moving in opposite directions. Figure 1 shows the collected shot with the interference of the two vessels marked with 'D' and 'E' and timing differences between the consecutive guns.

STARTING MODEL BUILDING, VALIDATION AND DATA PRECONDITIONING

The initial model was obtained from the legacy model that was built using a traditional top-down approach using the underlying streamer data that comprises 8–16 km maximum offset. Prior to the final starting model derivation, we applied full-waveform inversion (FWI) to run scenarios using the streamer data to improve the questionable salt geometries, which can be very beneficial to delineate the complex top of salt and form the flanks. After smoothing the legacy model, FWI was employed to modify salt geometry and update the sedimentary section around the salt. The next step was to validate this

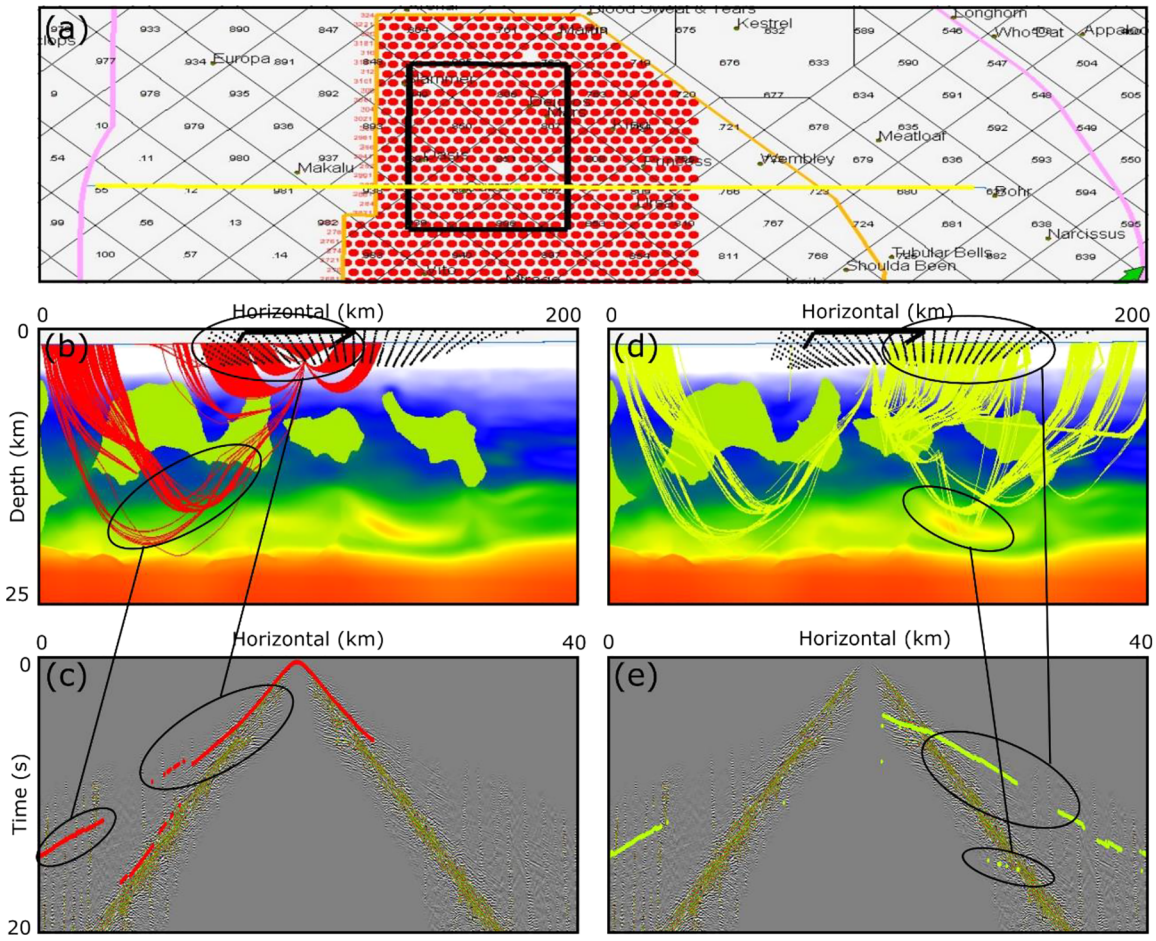

FIGURE 2 (a) Node location map; (b) early arrival ray tracing overlaid on the observed data based upon the initial velocity; (c) displaying the simple diving wave arrivals; (d) early arrival ray tracing overlaid on the observed data in complex area where deep carbonate is present in the model; (e) displaying the complex diving wave arrivals.

model, especially in the deep part around the autochthonous salt level, which is recorded by the longer offsets beyond 40 km. Based upon regional 2D studies, we adjusted the deep part of the model by placing an increased velocity gradient from the top Oligocene onwards, and another from the base Louann salt onwards. Early-arrival ray tracing and data fitting QCs were used for the validation steps. The ray tracing showed a reasonably good match on the far offset, which may mitigate cycle skipping in the deep part of the model. Figure 2 shows the ray tracing validation result.

The FWI input data was the blended one for two reasons first is to safely preserve the low frequencies and the second is to have a very early start of the FWI not to wait on the deblending. The deblending is a multi-stage strategy where different sparsity promoting prior information are utilized to optimize the signal-to-noise ratio at each stage. In each stage, the algorithm focuses on separating different modes of seismic signal starting with the strongest signal. This deblending method is called multi-stage iterative source separation with priors (Kumar et al., 2023). After deblending, there was PZ summation to create the input data for imaging purpose. The imaging used 20 km maximum offset from the sparse-node data.

FULL-WAVEFORM INVERSION APPLICATION FOR VELOCITY MODEL BUILDING

Although the first convincing applications of 3D full-waveform inversion (FWI) were performed with stationary-receiver as Ocean Bottom Cable (OBC) geometry (Plessix & Perkins, 2010; Sirgue et al., 2010), many applications are currently performed with towed-streamer data especially for exploration purpose. The drawback of such acquisition is the limited length of the streamer which prevents deep targets from being sampled by diving waves and post-critical reflections for FWI. This issue has been partly bypassed by adapting FWI to reflection data leading to the so-called reflection-based waveform inversion (RWI) (Brossier et al., 2014; Xu et al., 2012). RWI relies on the scale

separation between the reflectivity and the velocity macro-model underlying classical reflection processing workflow based upon alternated migration and migration-based velocity analysis. To some extent, RWI breaks down the original FWI idea of continuously sampling the wavenumber spectrum of the subsurface by exploiting the rich angular illumination provided by wide-aperture acquisitions such as surface permanent receiver acquisitions (OBC, OBN, land) (Pratt et al., 1996). Today, long-offset multi-component node acquisitions emerge as an alternative to towed-streamer acquisition for deep-water offshore subsalt exploration. These stationary-receiver acquisitions offer the necessary versatility to design full-azimuth ultra-long offset acquisitions that are suitable to sample the full targeted structures with a wide variety of wave types in term of propagation regime (transmission vs. reflection), propagation direction. This provides an optimal setting to really exploit the resolution power of FWI and its ability to reconstruct all the physical parameters that govern wave propagation.

One of the most difficult parts of subsalt imaging is to build the correct salt geometry and define the salt velocity. The traditional standard practice for salt model building is to use tomography to first build the best possible sediment velocity model. After building, the background model in the shallow part, sediment flood and, later, salt flood is executed to interpret, first, the top of salt and then the base of salt in simple circumstances. The salt geometry building becomes more complex if several salt overhangs must be incorporated into the model. To delineate the complex salt shape, numerous salt scenarios may be performed to execute trial and error modification on the salt. This procedure is not only labour-intensive and time-consuming, but it is also subject to human errors. FWI is considered an effective data-driven technique to build velocity models by iteratively minimizing the difference between observed and predicted data.

The mismatch in the time-domain between the model and the observed data (Vigh et al., 2019) can be computed as local attributes as a function of displacement shift in X and possibly Y. Many approaches to solve the issues of cycle-skipping and amplitude discrepancy have been proposed (Luo & Schuster, 1991; Ma & Hale, 2013). If the time shift is calculated in one dimension, it is not taking the lateral shift into account due to the complexity of the model like salt diffraction energy can distorte the time shifts calculation. These techniques may determine a false time shift, which may lead to ambiguous velocity updates in complex areas.

In this context, FWI is able to match the local patterns between the observed and predicted shot record for both travel-time and spatial shifts. Moreover, the time shift (Jiao et al., 2015) can be computed as local attributes as a function of displacement.

Thus, FWI can directly minimize the travel-time shift objective function to back-project the local travel-time shift into the model. This traveltime is determined in a three-dimensional sense in complex salt-related geology to ensure proper pairing of the events between acquisition and prediction. After the travel-time shift reduces below the half cycle, then amplitude will play a role in the velocity updates. The enhanced template matching objective function has proven to be less sensitive to the cycle-skipping problem than the traditional least-square objective function, while retaining the ability to reshape complex salt geometry and the subsalt velocity trend if there is a long enough offset in the observed data;

$$E = \frac{1}{2}\sum_s \sum_r \int \mathrm{d}t \left(\left(d_{\mathrm{pred}}\left(\mathbf{x}_{\mathrm{s}}, \mathbf{x}_{\mathrm{r}}, t\right) - d_{\mathrm{obs}}\left(\mathbf{x}_{\mathrm{s}}, \mathbf{x}_{\mathrm{r}}, t\right)\right)^2 + \lambda \Delta T\left(\mathbf{x}_{\mathrm{s}}, \mathbf{x}_{\mathrm{r}}, t\right)^2 \right), \quad (1)$$

where d_{obs} are the observed data, and d_{cal} are the data calculated, respectively, t represents time and $\mathbf{x}_{\mathrm{s}}$ and $\mathbf{x}_{\mathrm{r}}$ denote the sources and receivers, respectively, using the elastic wave. ΔT is the shift between the observed and predicted data in the 2D or 3D window depending upon the receiver sampling. The λ is a dimensioning parameter used to adaptively balance the contributions from the kinematic and dynamic terms in the misfit function E Equation (1). Note the travel-time contribution diminished naturally as the background velocity is improved over iterations. This objective function addresses cycle skipping by resolving the travel-time minimization then emphasizes on the waveform matching in the least squares part of minimization.

After confirming the validity of the initial model, the FWI was executed in a multi-scale manner starting around 1.7 Hz. However, 1.7 Hz was still not a low-enough frequency to discount the cycle-skipping possibility in the FWI due to the complex salt geometry. If the low frequencies are not enough to resolve the model, there is a requirement for model perturbation and to restart the FWI with the lowest frequency in the acquired data. Using the low-frequency updates, we managed to modify the salt and the subsalt velocities to gain better kinematics, improving the deep velocity field for subsalt imaging. We gradually increased the frequencies in the FWI to reach the 16 Hz mark to see how the high-frequency FWI updates impact the salt geometry and the subsalt velocity that influence the imaging for exploration and development proposes. Figure 3 demonstrates the image improvements that are the result of the FWI fine-tuned velocity model.

Figure 3b shows the updated FWI velocity and the impact on imaging of this velocity update versus the legacy velocity and its image in Figure 3a. The subsalt sediment and the deep base Louann were put together very coherently with the velocity that was coming from the FWI-only updates. The increase in imaging quality is attributed to the long-offset, full-azimuth, OBN acquisition that unlocked the potential of the FWI to develop the velocity field. The kinematics of the deep section improved significantly compared to the initial model, which can be observed in Figure 4b versus (a).

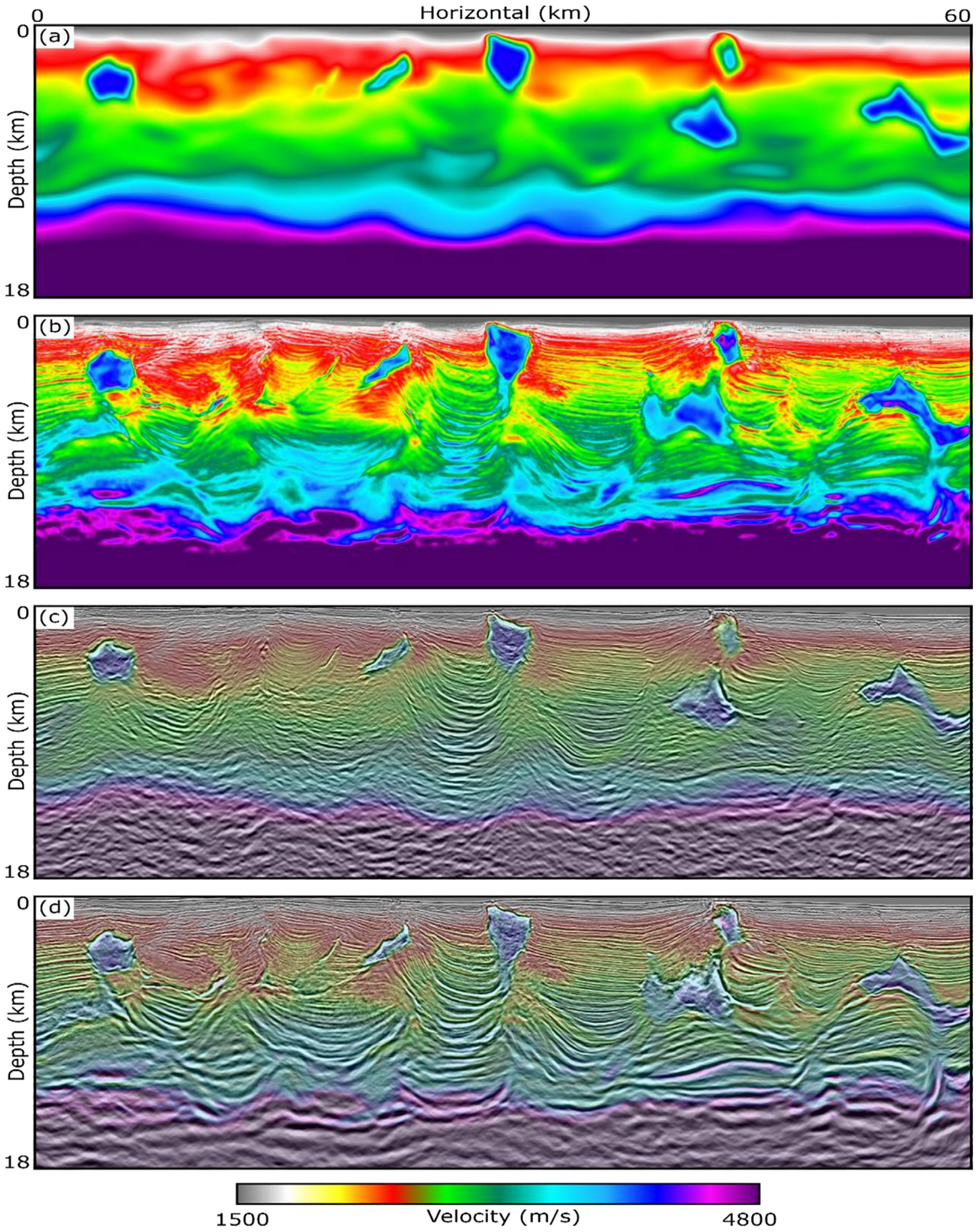

FIGURE 3 (a) Legacy/initial velocity field; (b) full-waveform inversion (FWI)-updated velocity; (c) legacy/initial velocity and its image with ocean-bottom node (OBN) input data; (d) FWI-updated velocity and its image with OBN data.

Eventually, we can extract the pseudo-reflectivity from the FWI updated the structural tensor velocity field, which is a three-dimensional first derivative of the velocity, considering the dip field obtained from the imaging algorithm at the stage of the extraction. When the frequencies increase in the FWI, the updates show high resolution details that allow us to extract the reflectivity with the following equation:

$$\frac{\partial I}{\partial \mathbf{n}} = \frac{\partial I}{\partial x}\sin\theta\cos\varphi + \frac{\partial I}{\partial y}\sin\theta\sin\varphi + \frac{\partial I}{\partial z}\cos\theta, \qquad (2)$$

where θ, φ are the dip and the rotation information in the in-line/crossline orientation derived from the migrated image, $\mathrm{d}x, \mathrm{d}y, \mathrm{d}z$ are the three-dimensional derivatives, and I is the impedance that can be extracted

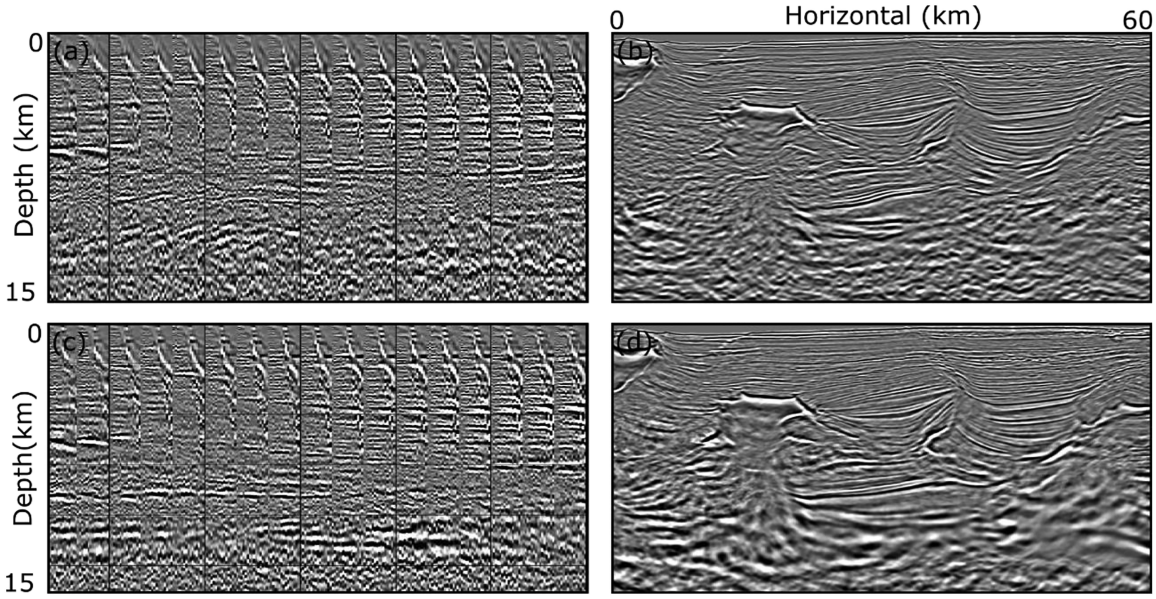

FIGURE 4 (a) Initial velocity reverse-time migration (RTM) gathers; (b) initial model RTM image; (c) full-waveform inversion (FWI) model produced RTM gathers; (d) FWI model produced RTM image.

from the relatively high frequency FWI updated velocity.

This volume has two major differences compared to an RTM image; one is the full wavefield that goes into FWI, and the other one is the iterative nature of FWI, which acts like a non-linear least squares RTM. Using the full wavefield can extend the illumination of the subsalt sedimentary section due to the diving waves and multiples contribution, whereas iterating with FWI can improve resolution compared to the RTM image that utilizes only the primary reflections. Furthermore, one can say the fair comparison would be the least-squares RTM which is iterative though but uses reflection primary data too with a Born-modelling engine. Figure 5a shows the high frequency FWI updated velocity field, whereas part (b) shows the extracted FWI derived reflectivity.

INCREASED PHYSICS IN FULL-WAVEFORM INVERSION APPLICATION

The recent successful applications of time-domain elastic FWI (EFWI) include Vigh et al. (2014) using four component data, Plessix et al. (2021) in salt environment and Wang et al. (2021) where amplitude versus offset class II presented in the geology, in which the acoustic propagation results in false prediction. These previous exercises update V_p and V_s, whereas others use the V_s as a relationship to V_p to update the pressure velocity field only. We show that the V_p only update, with a proportional V_s, still gives tremendous uplifts in complex geology.

Even so, node spacing may become a limiting factor for EFWI application towards high frequencies due to the slower S-velocity relative to P-velocity and especially in S-velocity inversion from the horizontal components. These are main factors governing OBN acquisition design in terms of FWI and should be analysed if the S-velocity inversion is targeted.

In this study, the initial model was obtained from a legacy model that was built with the traditional top-down approach. After smoothing the legacy model, FWI (acoustic) was employed to update the entire model including the salt geometry and sedimentary section above and below the salt. After confirming the validity of the initial model with rigorous QCs, the EFWI was executed in the multi-scale manner starting from 1.7 Hz. The frequency marching increment was 1 Hz at the low end to avoid the possibility of getting trapped in local minima and exhausting most of the low frequencies in the observed data. The maximum frequency of the EFWI was 6 Hz that already gave us a very good imaging uplift. We have executed both acoustic and EFWI in parallel to see if our observations in the real field data example, and if the benefit of the increased physics in FWI is evident in these results. Using the low-frequency updates, we succeeded in modifying the salt and the subsalt velocities to gain better kinematics that improve the deep velocity field, as well as images for subsalt regions in both acoustic and EFWI (Vigh et al., 2022). Some observations can be drawn after finishing the low-frequency updates. Figure 6d shows that the EFWI results have more geological consistency compared to the acoustic result in Figure 6b.

The update of the velocity in the top of salt from EFWI (Figure 6d) shows the velocity slowing down instead of

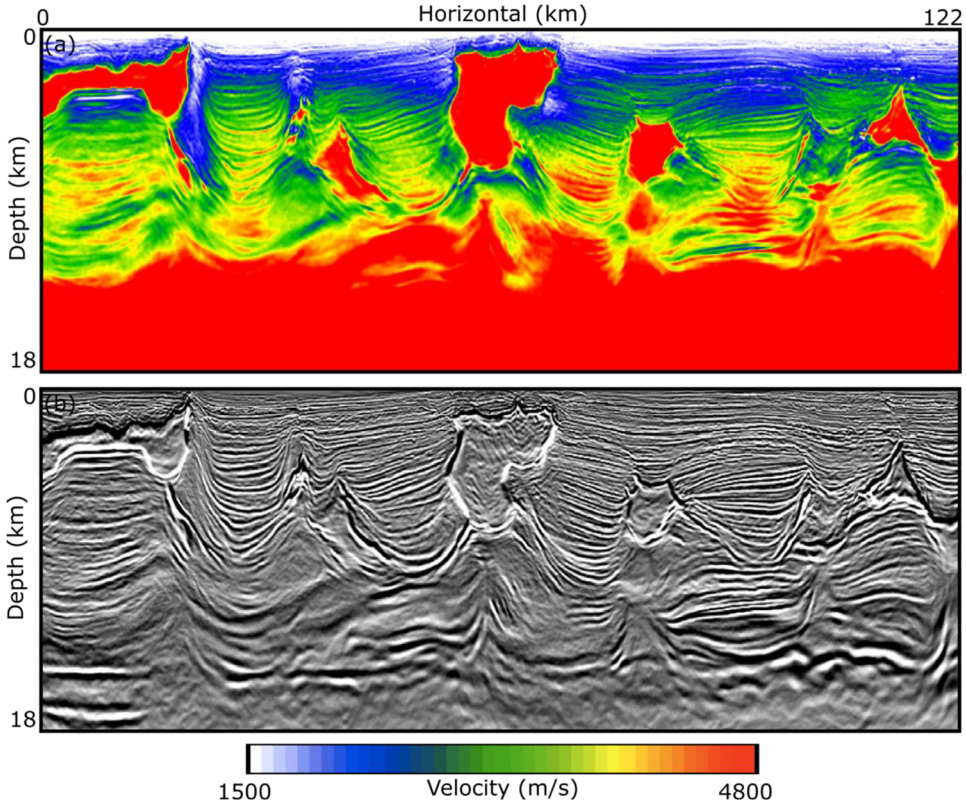

FIGURE 5 (a) Full-waveform inversion (FWI) updated velocity; (b) extracted pseudo-reflectivity from the FWI velocity.

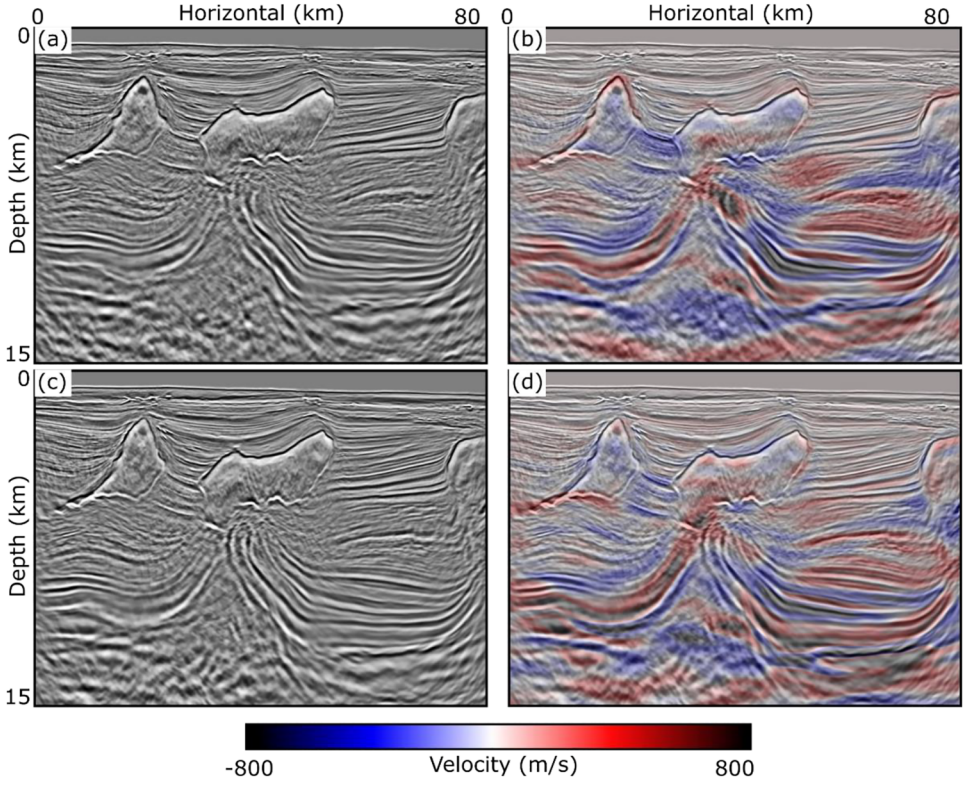

FIGURE 6 (a) Acoustic full-waveform inversion (FWI) image with ocean-bottom node (OBN) input data; (b) acoustic FWI perturbation with its image with OBN data; (c) elastic FWI image with the OBN input data; (d) elastic FWI perturbation with its image with OBN data.

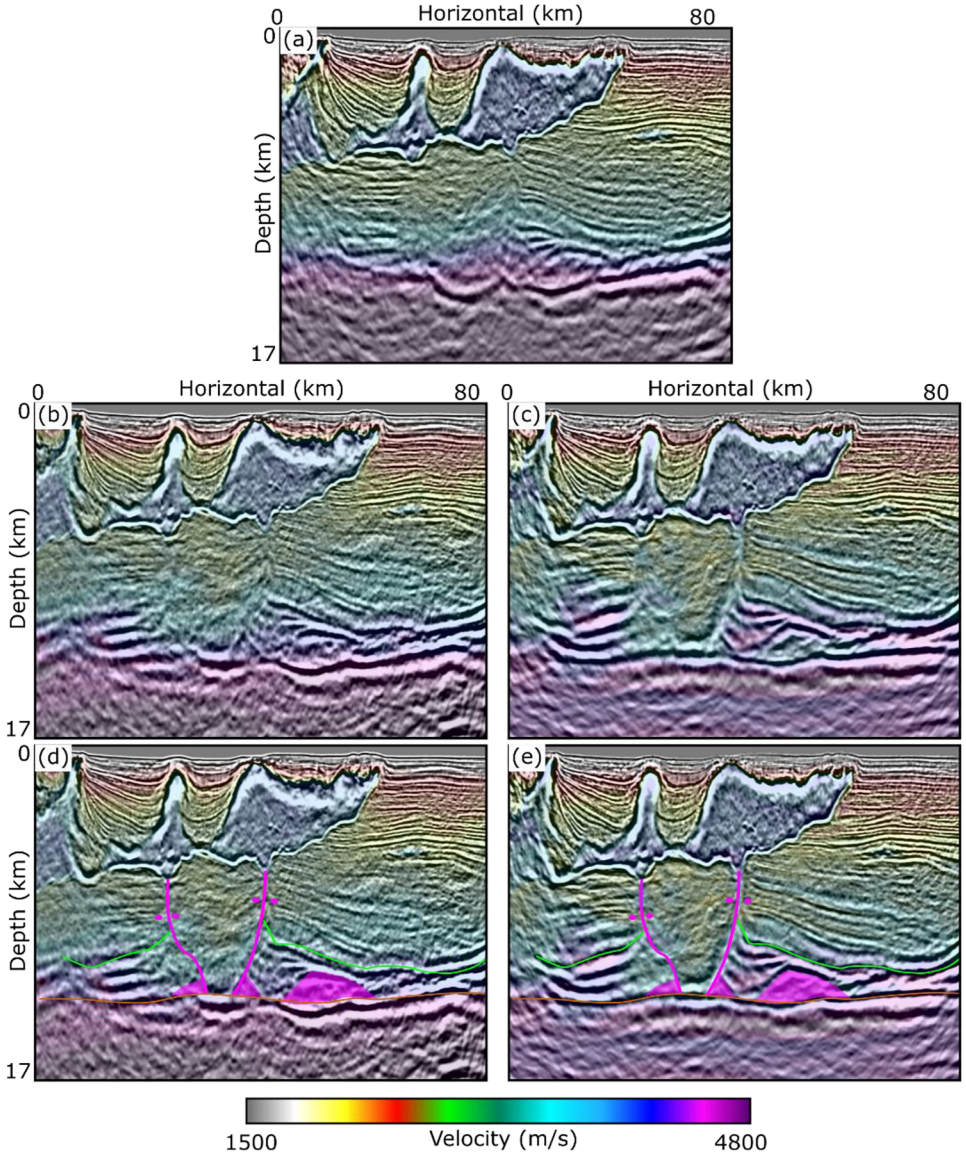

FIGURE 7 (a) Initial model and its image; (b) acoustic full-waveform inversion (FWI) velocity and its image overlay; (c) elastic FWI velocity and its image overlay; (d) acoustic FWI updates overlain on its image with interpretation; (e) elastic FWI updates overlain on its image with interpretation.

speeding up as shown in the acoustic FWI update (Figure 6b). This velocity decrease in sediment above the top of salt is in fact the right direction due to the smoothness in the initial model. The subsalt update is less patchy in the EFWI, and this can be attributed to the better amplitude handling from the elastic consideration. Last, but not least, the steeply dipping events and salt feeders in the image from the EFWI updated model (Figure 7e) are more pronounced than those in the counterpart image using the acoustic FWI updated version (Figure 7b), which suggests that the EFWI could generate better model updates than acoustic FWI. Both inversions returned improvements when their results are compared to the initial model image as shown in Figure 7a. However, when the interpretation is carried out on the EFWI image, mapping of the welding system and the Top Cretaceous is improved on the EFWI image (Figure 7e). We overlaid markers on the acoustic FWI image to demonstrate the accuracy of the EFWI, in that the sedimentary section terminations are more visible in the EFWI image.

CONCLUSION

The results support the proposition that long-offset, full-azimuthal sparse ocean-bottom node acquisition is a viable data collection technique for regional studies, especially to derive an accurate velocity field by full-waveform inversion (FWI). The FWI workflow enabled building a velocity

model in this extraordinarily complex salt geology environment, and FWI showed its ability to reshape salt geometry automatically and update the deep model without requiring major human intervention. The improvement in the salt and sediment velocity field resulted in superior subsalt imaging and better understanding of the deep geologic trends. Elastic FWI (EFWI) generates better P-velocity updates around salt and in the subsalt areas, compared to acoustic FWI. By taking more realistic physics into the simulation and inversion, EFWI resulted in more reliable velocities in complex areas and the images show better delineated salt geometries, more focused continuous steep-dip events and more geological consistencies. Even though the computational cost can still be significantly more expensive than acoustic propagators, it has become feasible to run EFWI for 3D surveys within a reasonable time frame.

ACKNOWLEDGEMENTS

The authors thank WesternGeco Multiclient and TGS for permission to show and publish this work.

DATA AVAILABILITY STATEMENT

The data cannot be shared in the paper.

REFERENCES

Brossier, R., Operto, S. & Virieux, J. (2014) Velocity model building from seismic reflection data by full-waveform inversion. *Geophysical Prospecting*, 63(2), 354–367.

Brossier, R., Operto, S., & Virieux, J. (2010). Robust Frequency–domain Multi–parameter Elastic Full Waveform Inversion. *72nd EAGE Conference and Exhibition Incorporating SPE EUROPEC 2010*. https://doi.org/10.3997/2214–4609.201400802

Castellanos, C., Etienne, V., Hu, G., Operto, S., Brossier, R., & Virieux, J. (2011). Algorithmic and methodological developments towards full waveform inversion in 3D elastic media. *SEG Technical Program Expanded Abstracts 2011*. https://doi.org/10.1190/1.3627774

Crase, E., Pica, A., Noble, M., Mcdonald, J. & Tarantola, A. (1990) Robust elastic nonlinear waveform inversion: application to real data. *Geophysics*, 55, 527–538.

Djikpéssé, H.A. & Tarantola, A. (1999) Multiparameter L1 norm waveform fitting: interpretation of Gulf of Mexico reflection seismograms. *Geophysics*, 64, 1023–1035.

Fichtner, A. & Trampert, J. (2011) Resolution analysis in full waveform inversion. *Geophysical Journal International*, 187(3), 1604–1624.

Huang, X., Eikrem, K.S., Jakobsen, M. & Nævdal, G. (2020) Bayesian full-waveform inversion in anisotropic elastic media using the iterated extended Kalman filter. *Geophysics*, 85(4), C125–C139.

Jiao*, K., Sun, D., Cheng, X., & Vigh, D. (2015). Adjustive full waveform inversion. *SEG Technical Program Expanded Abstracts 2015*. https://doi.org/10.1190/segam2015–5901541.1

Kalita, M., Kazei, V., Choi, Y. & Alkhalifah, T. (2019) Regularized full-waveform inversion with automated salt flooding. *Geophysics*, 84(4), R569–R582.

Kumar, R., Kamil, Y., Bilsby, P., Narayan, A., Mahdad, A., Brouwer, W.G., Misbah, A., Vassallo, M., Zarkhidze, A. & Watterson, P. (2023) Inversion-based multistage seismic data processing with physics-driven priors. *The Leading Edge*, 42(1), 52–60.

Li, Q., Slopey, W., Rollins, F., Billette, F., Udengaard, C. & Thompson, B.J. (2019) Leading a new deep water OBN acquisition era: two 2017–2018 GoM OBN surveys. In *SEG international exposition and annual meeting*. SEG.

Luo, Y. & Schuster, G.T. (1991) Wave-equation traveltime inversion. *Geophysics*, 56(5), 645–653.

Ma, Y. & Hale, D. (2013) Wave-equation reflection traveltime inversion with dynamic warping and full-waveform inversion. *Geophysics*, 78(6), R223–R233.

Nolte, B., Rollins, F., Li, Q., Dadi, S., Yang, S., Mei, J., & Huang, R. (2019). Salt velocity model building with FWI on OBN data: Example from Mad Dog, Gulf of Mexico. *SEG Technical Program Expanded Abstracts 2019*. https://doi.org/10.1190/segam2019–3216777.1

Plessix, R.-E. & Perkins, C. (2010) Thematic set: full waveform inversion of a deep water ocean bottom seismometer dataset. *First Break*, 28(4), 71–78.

Plessix, R.-É. & Krupovnickas, T. (2021) Low-frequency, long-offset elastic waveform inversion in the context of velocity model building. *The Leading Edge*, 40(5), 342–347.

Pratt, R.G., Song, Z.-M., Williamson, P. & Warner, M. (1996) Two-dimensional velocity models from wide-angle seismic data by wavefield inversion. *Geophysical Journal International*, 124(2), 323–340.

Ratcliffe, A., Bretherton, S., Xiao, B. & Haacke, R. (2019) High-frequency full-waveform inversion: just how high should you go? In: 81st EAGE *conference and exhibition workshop progra*mme, vol. 2019. EAGE. pp. 1–2.

Rocha, D., Tanushev, N., & Sava, P. (2016). Anisotropic Elastic Wavefield Imaging Using the Energy Norm. 78th EAGE Conference and Exhibition 2016. https://doi.org/10.3997/2214–4609.201601533

Sears, T. J., Barton, P. J., & Singh, S. C. (2010). Elastic full waveform inversion of multicomponent ocean–bottom cable seismic data: Application to Alba Field, U. K. North Sea. *GEOPHYSICS*, 75(6), R109–R119. https://doi.org/10.1190/1.3484097

Sirgue, L., Barkved, O.I., Dellinger, J., Etgen, J., Albertin, U. & Kommedal, J.H. (2010) Thematic set: full waveform inversion: the next leap forward in imaging at Valhall. *First Break*, 28(4), 65–70.

Vigh, D., Jiao, K., Watts, D. & Sun, D. (2014) Elastic full-waveform inversion application using multicomponent measurements of seismic data collection. *Geophysics*, 79(2), R63–R77.

Vigh, D., Cheng, X., Jiao, K., Xu, Z. & Dai, W. (2019) Is the salt-related full-waveform inversion sorted out? [Expanded abstracts]. In: *89th annual international meeting*. SEG. pp. 1265–1269.

Vigh, D., Cheng, X., Xu, Z., Jiao, K. & Brand, N. (2020) Sparse-node long-offset velocity model building in the Gulf of Mexico [Expanded abstracts]. In: *90th annual international meeting*. SEG. pp. 706–709.

Vigh, D., Xu, J., Cheng, X. & Bai, B. (2022) Elastic full-waveform inversion using OBN data acquisition. In *SEG/AAPG international meeting for applied geoscience & energy*. OnePetro.

Vigh, D., Jiao, K., Cheng, X., Sun, D., & Lewis, W. (2016). Earth–model building from shallow to deep with full–waveform inversion. *The Leading Edge*, 35(12), 1025–1030. https://doi.org/10.1190/tle35121025.1

Virieux, J. & Operto, S. (2009) An overview of full-waveform inversion in exploration geophysics. *Geophysics*, 74(6), WCC1–WCC26.

Wang, H., Burtz, O., Routh, P., Wang, D., Violet, J., Lu, R. & Lazaratos, S. (2021) Anisotropic 3D elastic full-wavefield inversion to directly estimate elastic properties and its role in interpretation. *The Leading Edge*, 40(4), 277–286.

Wu, R.-S., Luo, J. & Wu, B. (2014) Seismic envelope inversion and modulation signal model. *Geophysics*, 79(3), WA13–WA24.

Xu, S., Chen, F., Lambaré, G., Zhang, Y. & Wang, D. (2012) Inversion on reflected seismic wave [Expanded abstracts]. In: *82nd annual international meeting*. SEG. pp. 1–7.

How to cite this article: Vigh, D., Xu, J., Cheng, X. & Glaccum, K. (2023) Sparse-node acquisition for data fitting velocity model building. *Geophysical Prospecting*, 1–11. https://doi.org/10.1111/1365-2478.13393